Potential ASR expansion mitigation of ferronickel slag aggregate by fly ash

Ashish Kumer Saha[1*], Prabir Kumar Sarker[2]

[1]PhD student, Department of Civil Engineering, Curtin University, GPO Box U1987, Perth, WA 6845, Australia.

[*]Corresponding author, Email: a.saha@postgrad.curtin.edu.au

[2]Associate Professor, Department of Civil Engineering, Curtin University, GPO Box U1987, Perth, WA 6845, Australia.

Email: P.Sarker@curtin.edu.au

Synopsis

This study investigates the potential alkali silica reaction (ASR) of ferronickel slag (FNS) aggregate, which is a by-product of nickel production. A class F fly ash was used as a possible ASR mitigation in accelerated mortar bar test (AMBT) specimens containing 50% FNS. There were visible surface cracks on the specimens using no fly ash or 10% fly ash. Use of 20% fly ash reduced expansion by 45% as compared to that with 10% fly ash. In accordance with the expansion limits of Australian Standard, the mixtures using 20% and 30% fly ash were categorised as slowly-reactive and non-reactive, respectively. Thermogravimetric analysis (TGA) and microstructural observations confirmed the effectiveness of fly ash in reducing Portlandite content that reduced the ASR expansion. Therefore, the use of 20% to 30% fly ash as cement replacement is considered as an adequate ASR mitigating measure of FNS fine aggregate.

KEYWORDS Accelerated mortar bar test, alkali silica reaction, ferronickel slag, fly ash.

1 Introduction

Concrete is the most highly used material after water. The demand for concrete is increasing by 6% every year due to the massive infrastructure growth in developing countries [1]. Concrete production requires an enormous amount of natural resources such as sand, stone and water. Fine aggregate is an essential part of concrete as it not only fills the void but also provides the rigidity to concrete. Therefore, good quality fine aggregate is essential for the production of good concrete. Natural sand has been used as the common fine aggregate in concrete and mortar. As a result, excessive and uncontrolled river mining has been observed not only in developing countries but also in developed countries like Australia [2]. It has been well established that excessive sand extraction from river bed can lead to disruption of the aquatic eco-system [3]. In addition, unplanned river-dredging increases the failure risk of waterfront structures [4]. Similarly, excessive sand quarrying from hills increases the risk of landslides [5]. Thus, the utilisation of industrial by-products such as FNS as a partial or full replacement of natural sand can help sustainable infrastructure development.

Alkali silica reaction (ASR) is an important durability issue of concrete produced using reactive aggregates. The reaction of reactive siliceous aggregate with the alkali present in binder leads to formation of an expansive gel and imparts swelling pressure that may cause cracking and strength loss of concrete structures [6-7]. Stanton [8] first identified this deleterious expansion in concrete. Extensive research has been carried out since then on the mitigation of this durability issue. There are different kinds of reactive aggregates that can be found in nature or as industrial by-products, such as cristobalite, opaline silica, volcanic

glasses, cryptocrystalline quartz, strained quartz, chalcedony, nickel slag and spratt [9-11]. The chemical reactions that take place in ASR can be expressed by Eqs. 1-3 [12-13]. It can be seen that at the initial stage of ASR, the alkali ion (R^+) from pore solution attacks the reactive silica (≡Si-O-Si≡) and generates alkali silicate (Si-O-R) gel and silicic acid (Si-OH). Afterwards, the silicic acid again reacts with the alkali and generates more alkali silicate. At the final stage, this gel absorbs water from the pore solution and expands in volume. The volume expansion imparts swelling pressure to the surrounding concrete. The presence of calcium ion (Ca^{2+}) plays an important role in ASR. It acts as a buffer to maintain alkalinity of the pore solution [14]. Dron and Brivot [15] observed that calcium ion reacts with the alkali-silicate gel at the final stage of ASR and produces alkali-calcium-silicate-hydrate (R-C-S-H).

$$\equiv Si\text{-}O\text{-}Si\equiv + OH^- + R^+ \rightarrow \equiv Si\text{-}O\text{-}R + H\text{-}O\text{-}Si\equiv \quad (1)$$

$$\equiv Si\text{-}O\text{-}H + OH^- + R^+ \rightarrow \equiv Si\text{-}O\text{-}R + H_2O \quad (2)$$

$$\equiv Si\text{-}O\text{-}R + nH_2O \rightarrow \equiv Si\text{-}O^- \text{ -- } (H_2O)_n + R^+ \quad (3)$$

In order to mitigate the ASR expansion, different types of supplementary cementing material (SCM) has been studied extensively over the past decades. SCMs can bind the free alkali and reduce alkalinity of the pore solution that is required for ASR to take place [16, 17]. Therefore, the use of fly ash and ground granulated blast furnace slag (GGBFS) has been found to reduce ASR expansion [18]. The chemical composition of an SCM can significantly influence its effectiveness to reduce ASR. It was observed that high alkali and high calcium fly ash (class C fly ash) are less effective in mitigation of ASR expansion as compared to low alkali and low calcium fly ash [19, 20]. However, Turk et al. [21] argued that the use of a class F fly ash up to 30% as an SCM was not enough to reduce the ASR of reactive aggregates found in Turkey. Therefore, the type and dosage of an SCM can significantly affect the ASR of reactive aggregates.

Due to low grade of nickel ores found in the earth, a significant amount of slag is produced as by-product in the production process of ferronickel alloy. FNS aggregate consists of high density and low absorption particles that makes it a suitable alternative to natural sand in concrete. Chemical analysis showed that FNS contains a high amount of magnesium. When used in the form of ground fine powder, the hydration reaction of magnesium oxide may lead to formation of brucite and cause expansion over a period of time [22]. However, it was found that the magnesium of this FNS is bound in a crystalline structure known as forsterite, which is chemically stable and does not take part in hydration reaction [23]. Our previous studies [24, 25] showed that the use of FNS fine aggregate as 50% replacement of natural sand resulted in well grading of aggregate and maximum compressive strength with good workability of mortar and concrete. Therefore, this aggregate combination has been used to study the effect of different percentages of fly ash on the ASR of FNS aggregate. Fly ash was used as partial replacement of cement from 10% to 30% and its effectiveness to mitigate ASR has been investigated using accelerated mortar bar tests. Microstructural studies by scanning electron microscopy (SEM) and energy-dispersive X-ray spectroscopy (EDS), and TGA were carried out in order to understand the effect of fly ash percentage on ASR.

2 Experimental work

2.1 Materials

The binders used in this study were commercially available ordinary Portland cement (OPC) and a class F fly ash. The FNS fine aggregate was a by-product of the smelting of garnierite

nickel ore which is granulated by seawater cooling and then rain-washed on stockpiles. The chemical compositions of FNS, cement and fly ash, as determined by X-ray fluorescence (XRF), are given in **Table 1**. It can be seen that the main elements of FNS are silicon, magnesium and iron. The fly ash consisted of high amounts of silica and alumina with very low calcium. The type of OPC was general-purpose cement.

Table 1 Chemical compositions of OPC, FNS and fly ash (mass %)

Element	OPC	FNS	Fly ash
SiO_2	20.29	53.29	76.34
Al_2O_3	5.48	2.67	14.72
Fe_2O_3	2.85	11.9	3.69
MgO	1.24	31.6	0.54
SO_3	2.49	-	0.11
CaO	63.11	0.42	0.60
Na_2O	0.29	0.11	0.19
K_2O	0.45	-	0.96
Cr_2O_3	0.02	1.08	-
P_2O_5	0.17	-	0.10
SrO	0.05	-	-
TiO_2	0.27	-	0.61
Mn_2O_3	0.08	-	0.07
ZnO	0.04	-	-
NiO	-	0.1	-
Co_3O_4	-	0.01	-
LOI[a]	3.39	0.83	0.53

[a] loss on ignition.

The scanning electron microscope (SEM) images of cement and fly ash particles are shown in **Figure 1**. It can be seen that fly ash consists of spherical particles and OPC consists of angular particles of varying sizes.

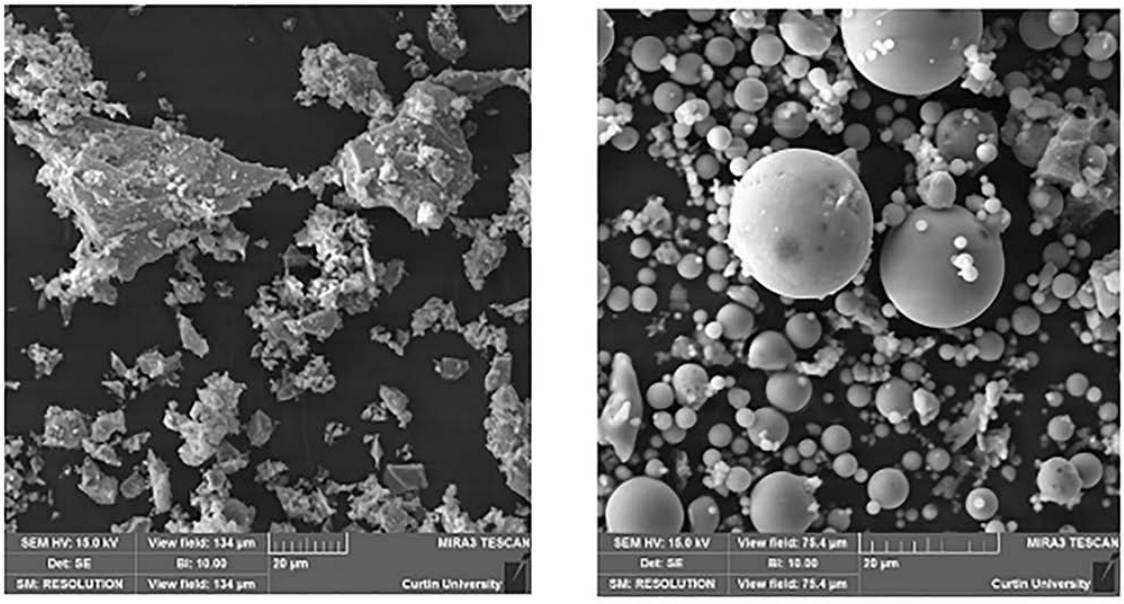

a. OPC b. Fly ash

Figure 1 SEM images of binders

The physical appearances of FNS and natural sand are shown in **Figure 2**. It is noticeable that FNS particles are relatively coarse and angular as compared to smaller and round sand particles.

a. Sand b. FNS

Figure 2 Physical appearance of aggregates

The microstructures of FNS and sand particles, as observed by SEM imaging, are shown in **Figure 3**. It can be seen that there are more micropores in FNS particles than in sand particles.

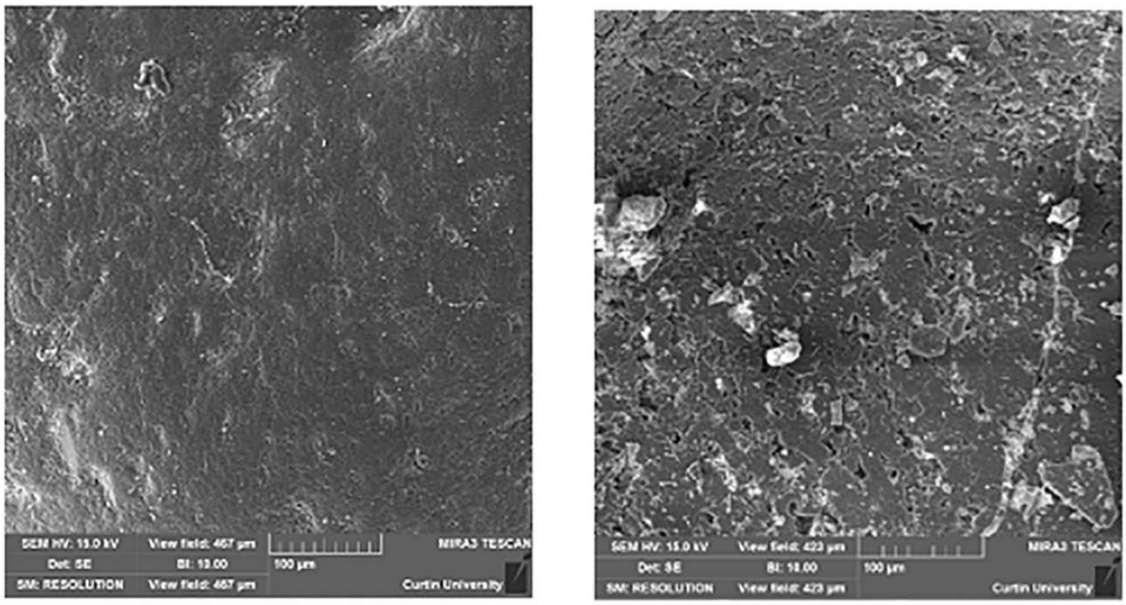

a. Sand b. FNS

Figure 3 SEM images of aggregates

The physical properties of aggregates are given in **Table 2**. It can be seen that the values of density, voids ratio and fineness modulus are higher for FNS aggregate than for natural sand. Due to the higher micropores, the water absorption of FNS is slightly higher than that of sand. Due to the higher angularity, the FNS particles did not flow in the sand flow cone

test and resulted in a higher voids ratio of the aggregate. The coarseness of FNS aggregate is reflected by its higher fineness modulus as compared to that of natural sand.

Table 2 Physical properties of aggregates

Property	Sand	FNS
SSD density (kg/m^3)	2160	2780
Apparent particle density (kg/m^3)	2320	2850
Fineness modulus	1.95	4.07
Water absorption	0.35	0.42
Uncompacted voids ratio (%)	32.42	44.39
Flow cone time (s)	17.19	DF

2.2 Methods

The mortar mix proportions are given in **Table 3**. The control mix consisted of 100% cement as the binder and is designated by OPC100. The other three mixes contained 10%, 20% or 30% fly ash, and are designated by FA10, FA20 and FA30, respectively. The ASR expansions of FNS aggregate with different percentages of fly ash were determined by accelerated mortar bar tests (AMBT) in accordance with the Australian standard [26]. Though the standard suggests a test period of 21 days, it was extended up to 64 days in order to evaluate any slow reactivity associated with the FNS. Mortar mixtures were prepared with a water to binder ratio of 0.47 and aggregate to binder ratio of 2.25, in accordance with the test standard.

Table 3 Mortar mixture proportions

Mix ID	Binder (kg/m^3)		Fine aggregate (kg/m^3)		W/C
	OPC	FA	Sand	FNS	
OPC100	602	-	678	678	0.47
FA10	541.8	60.2	678	678	
FA20	481.6	120.4	678	678	
FA30	421	181	678	678	

Fifty mm cube specimens were cast for compressive strength and porosity tests. The specimens were demoulded at 24 hours after casting and cured in lime-saturated water. Compressive strengths were tested at 7, 28 and 56 days of age. Porosity was determined by measuring the volume of permeable voids according to the ASTM standard [27]. After 28 days of curing, the specimens were oven dried at 110 ^{o}C for a period of 3 days to reach the mass equilibrium and then submerged in water for 48 hours. The saturated surface dry (SSD) weight of the sample was then determined. Porosity was calculated by using these mass values of the specimen.

The AMBT specimens consisted of 25×25×275 mm mortar bars with studs inserted at the ends. The specimens were cured in hot water bath at 80 ^{o}C for 24 hours after demoulding and the initial length reading was taken using a length comparator. The specimens were then kept in 1M sodium hydroxide bath at 80 ^{o}C for 64 days and the length measurements were

conducted at time intervals given in the AS 1141.60.1 standard. Furthermore, cube specimens were subjected to the same exposure condition and compressive strengths were determined at 7, 28 and 56 days to evaluate the effect of the AMBT exposure on compressive strength.

Thermogravimetric analyses (TGA) were carried out on hardened cement pastes containing no fly ash (OPC 100), 10% fly ash (FA10), 20% fly ash (FA20) and 30% fly ash (FA30). The water-binder ratio was kept constant at 0.47 to make it consistent with the mortar mixes used for AMBT. The paste specimens were cured in water at 80 ^{o}C for 24 hours following by 21 days of immersion in 1M NaOH solution at 80 ^{o}C, which is same as the AMBT exposure. The samples were then ground and heated from room temperature to 800 ^{o}C under a nitrogen atmosphere to conduct TGA. This test was carried out in order to understand the effect of fly ash percentage on Portlandite content of the products produced in AMBT.

Microstructural investigation was carried out by scanning electron microscope (SEM) in order to evaluate the effect of fly ash on the ASR of FNS aggregate. Imaging was conducted after 21 days of exposure to the AMBT condition. The AMBT specimens were cut with a saw and representative samples were carbon coated for SEM image. The images were taken using a combination of secondary electron (SE) and backscattered electron (BSE) at an accelerating voltage of 15 kV. A combination of SE and BSE was adopted in order to observe the topography and identify different elements of the microstructure. Energy-dispersive X-ray spectroscopy (EDS) of selected points on the image was conducted in order to identify the reaction products.

3 Results

3.1 Compressive strength

An average compressive strength was determined from three identical specimens and the results are presented in **Table 4**. It can be seen that compressive strength gradually decreased with the increase of fly ash.

Table 4 Compressive strength of mortars containing 50% FNS fine aggregate

Mix ID	Compressive strength (MPa)		
	7 Days	28 Days	56 Days
OPC100	48	57	62
FA10	37	48	57
FA20	31	39	49
FA30	24	35	47

The control mixture exhibited high early strength of 48 MPa at 7 days that gradually decreased to 37 MPa, 32 MPa and 24 MPa for 10%, 20% and 30% fly ash, respectively. These are 78%, 64% and 50% of the 7-day strength of the control mixture. However, the pozzolanic reaction of fly ash enhanced strength development of the specimens at later ages. At 56 days of age, compressive strengths of the mortars FA10, FA20 and FA30 were 92%, 78% and 67% of the strength of control mixture, respectively. The fly ash contained high silica and low calcium that reduced the rate of hydration and strength at the early age. However, the presence of high silica content participated in pozzolanic reaction and formation of a secondary C-S-H gel that resulted in continued strength development beyond 28 days of age.

3.2 Porosity

Volume of permeable voids (VPV) test was carried out in order to determine the total porosity of hardened mortar specimens. Porosity of a specimen depends on the air voids, gel pores, capillary pores and microcracks (Andrews-Phaedonos 1996) [28]. The changes in VPV of mortar specimens with the increase of fly ash are plotted in **Figure 4**.

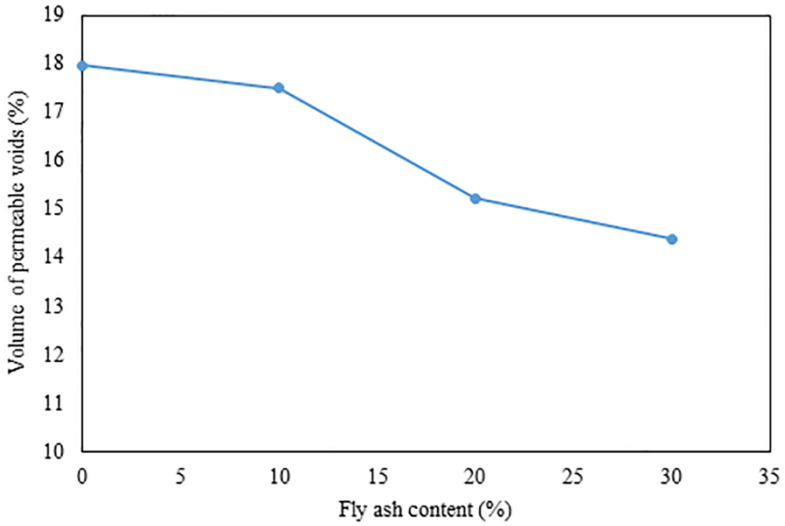

Figure 4 Volume of permeable voids of mortar with respect to fly ash percentage

It can be seen that porosity gradually decreased with the increase of fly ash. VPV of the control samples was 17.97% that decreased to 17.50%, 15.24% and 14.40% with the inclusion of 10%, 20% and 30% fly ash, respectively. Therefore, porosity decreased by 3%, 16% and 20% with the use of 10%, 20% and 30% fly ash, respectively. The reduction of porosity by the inclusion of fly ash is attributed to the densification of microstructure by pozzolanic reaction product and filling effect of the unreacted fly ash particles.

3.3 Accelerated mortar bar test results

Accelerated mortar bar test is a quick and effective method to identify the reactivity of aggregates. According to the Australian Standard AS 1141.60.1 [26], mortar bar expansions below 0.1% at the end of 21 days of the test are classified as nonreactive. When the 10-day expansion is below 0.1% and the 21-day expansion is between 0.1% and 0.3%, it is classified as slowly reactive. The 21-day expansion above 0.3% is classified as reactive. The accelerated mortar bar test (AMBT) is a part of different international standards such as, RILEM AAR-2 [29] and ASTM C1567 [30]. According to both these standards, expansion below 0.1% after 16 days of testing is classified as non-reactive and above 0.1% is classified as reactive.

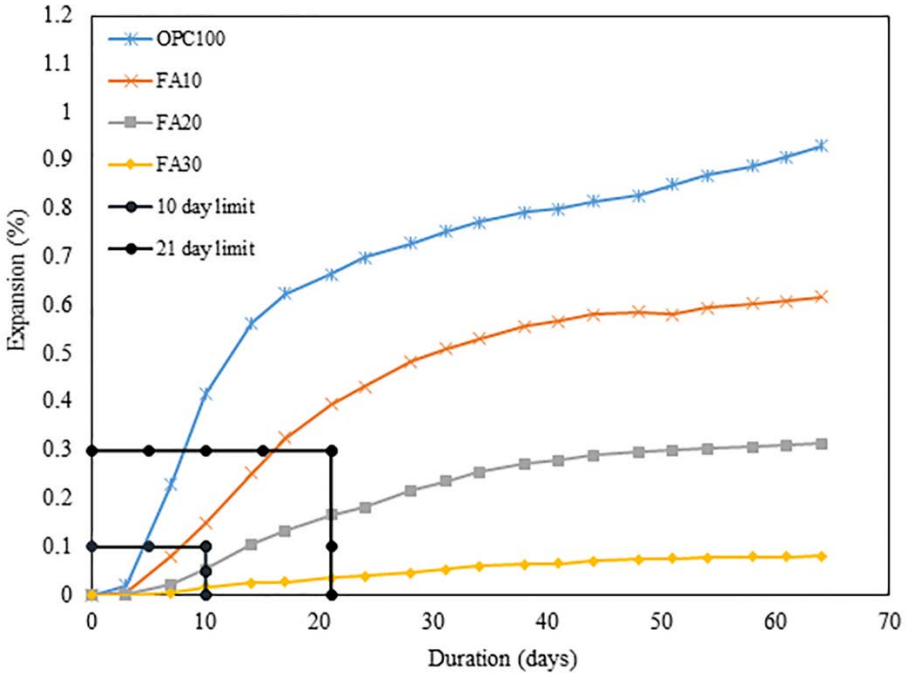

Figure 5 ASR expansion of mortar bars containing different percentages of fly ash

Expansions of the mortar bars containing 50% FNS aggregate and 50% sand with different proportions of fly ash are plotted in **Figure 5**. It can be seen that mix OPC100 experienced a significant expansion that was 0.930% at the end of 64 days of testing. It is also noticeable that expansion of the OPC100 specimens exceeded the 21-day limit of AS 1141.60.1. At the end of 21 days exposure, the expansion was 0.664%, which is more than twice the allowable limit. The use of 10% fly ash as cement replacement reduced expansion by 34% as compared to the control samples after 64 days of exposure. However, the expansion was above the allowable limit and it was in "reactive" category according to AS 1141.60.1. At the end of 21 days of exposure, the expansion of FA10 specimens was 0.392%. Furthermore, the 16-day expansions of OPC100 and FA10 was 0.624% and 0.326%, respectively. These values exceed the allowable limit of RILEM AAR-2 and ASTM C1567 standards. Therefore, both these mixes are classified as reactive in accordance with the limits of all three standards.

Expansion decreased by 66% as compared to that of the control specimens by the use of 20% fly ash in the binder. At the end of 10 and 21 days of exposure, the expansions were 0.056% and 0.167%, respectively, which is in "slowly reactive" category according to the Australian standard. The 16-day expansion of these samples was 0.131%, which is in the reactive category according to RILEM AAR-2 and ASTM C1567. Further increase of fly ash to 30% reduced expansion by 91% as compared to the expansion of the control specimens. The expansions after 10 and 21 days of exposure were 0.017% and 0.036%, respectively. According to AS 1141.60.1, these expansions are categorised as "non-reactive". The 16-day expansion of this sample was 0.028% which is in the non-reactive category according to RILEM AAR-2 and ASTM C1567.

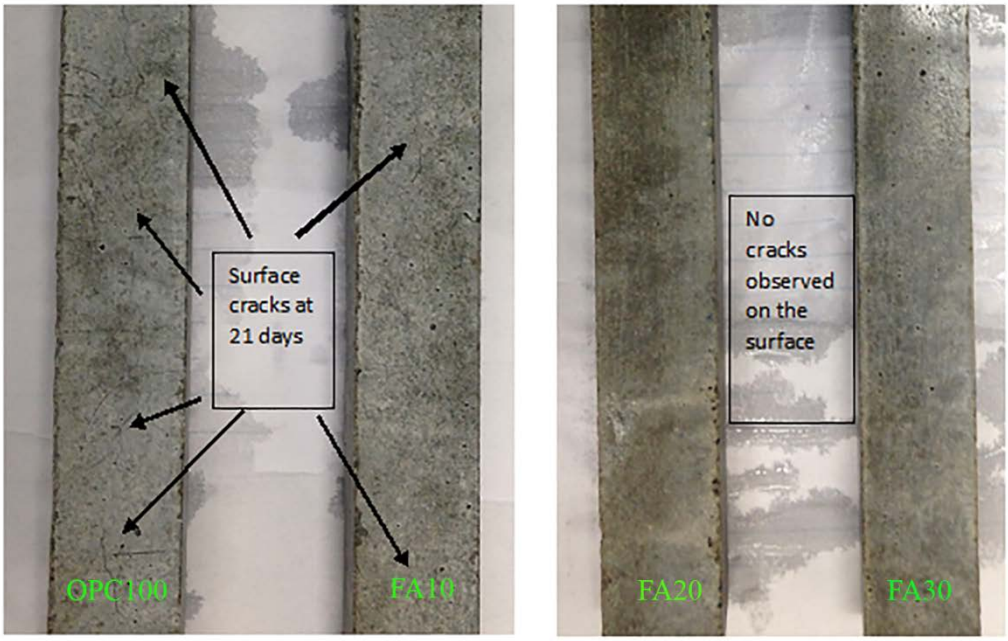

Figure 6 Visual inspection of AMBT samples after 21 days exposure

Photographs of the specimens at the end of 21 days of testing are presented in **Figure 6**. It can be seen that the specimens of mixtures OPC100 and FA10 experienced some visible cracks on the surface. This is consistent with the 10 and 21-day expansions that classified both the mixtures as "reactive. However, the number of cracks in specimens of FA10 were significantly less than in those in the specimens of OPC100. The specimens of FA20, which were classified as "slowly reactive" by the 10 and 21-day expansions, did not exhibit any surficial crack in the visual inspections. Also, the specimens of FA30, which were classified as "non-reactive", did not show any cracking on the surface. Therefore, the use of 30% class F fly ash as a SCM is considered adequate for mitigation of the expansion associated with 50% FNS as fine aggregate.

3.4 Effect of AMBT exposure on compressive strength

Compressive strengths of mortar cubes were determined after exposure to the AMBT test condition and the results are given in **Table 5**. It can be seen that the OPC100 and FA10 samples suffered 31% and 28% strength loss after 56 days of exposure, respectively.

Table 5 Effect of AMBT exposure on compressive strength of mortar samples

Mix ID	Compressive strength (MPa)			Change of strength (%)		
	7 Days	28 Days	56 Days	7 day	28 day	56 Days
OPC100	43	41	43	-10	-28	-31
FA10	34	37	41	-8	-23	-28
FA20	30	34	43	-3	-13	-12
FA30	25	38	51	4	9	9

On the other hand, the FA20 samples suffered a relatively low strength loss of 16%. The aggressive exposure of 1M NaOH at 80 ^{o}C resulted in the expansion and cracking of the OPC100 and FA10 samples, which were reflected by the significant strength losses. However, FA30 specimens exhibited strength gain rather than strength loss in the AMBT exposure. This is because 30% fly ash significantly reduced ASR of the FNS aggregates which is consistent with no cracking upon visual observations. In addition, the high-temperature exposure accelerated the pozzolanic reaction of fly ash. Thus, there was a relative strength improvement of 9% after 56 days of the exposure period.

3.5 Thermogravimetric analysis (TGA)

The TGA results are presented in **Figures 7(a)-7(d)**. The diagrams show the changes in mass of the specimen subjected to a progressive temperature increase. The DTA graph show three endothermic peaks. The initial peak was observed at 110 ^{o}C for OPC100 which is due to evaporation of the weakly bound water in calcium silicate hydrate (C-S-H) and ettringite [31, 32]. However, for the specimens containing fly ash, the initial peak was observed at around 150 ^{o}C. Thus, a comparison was made among the C-S-H contents of the specimens by measuring the mass losses in a temperature range of 45 ^{o}C to 150 ^{o}C. Thus, the C-S-H contents of specimens OPC100, FA10, FA20 and FA30 were found to be 6.42%, 6.37%, 5.23% and 4.98%, respectively. The calcium oxide contents of specimens containing fly ash decreased due to the replacement of OPC by fly ash. Thus, less C-S-H gel was formed in the fly ash blended cement pastes which also explains the low compressive strength of the fly ash mortar samples as compared to OPC100. The second peak was observed in the vicinity of 500 ^{o}C, which is due to the decomposition of portlandite (CH) [33, 34]. Therefore, a comparison is made to determine the portlandite content by measuring the mass loss at a temperature range of 450 ^{o}C to 550 ^{o}C. The CH content was 4.25%, 3.27%, 1.58% and 1.36% for the paste samples of OPC100, FA10, FA20 and FA30, respectively. Thus, cement replacement by fly ash reduced the CH content due to its pozzolanic reaction that eventually reduced the ASR of FNS aggregate. The third peak was observed in the vicinity of 760 ^{o}C which occurred due to the decomposition of calcium carbonate and release of carbon dioxide [35, 36].

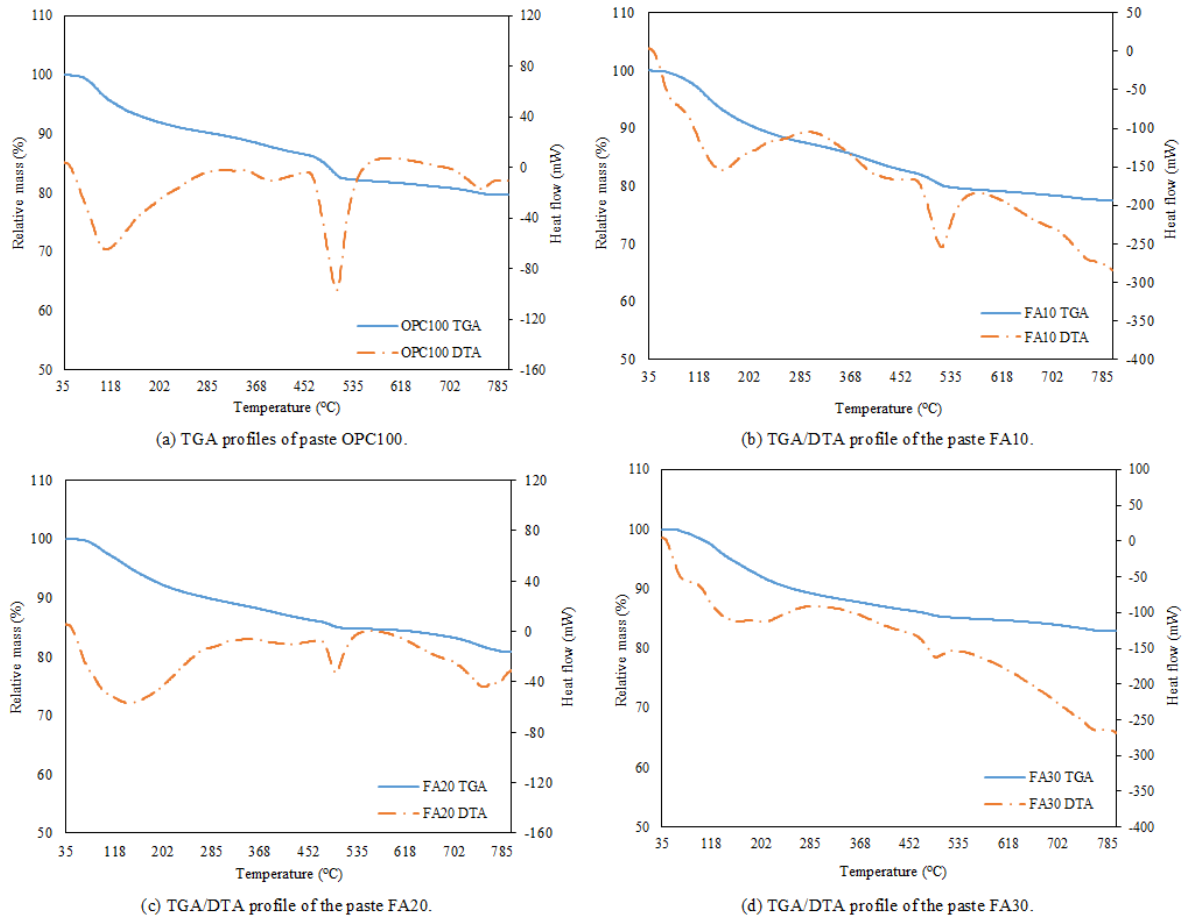

(a) TGA profiles of paste OPC100.

(b) TGA/DTA profile of the paste FA10.

(c) TGA/DTA profile of the paste FA20.

(d) TGA/DTA profile of the paste FA30.

Figure 7 Thermogravimetric mass changes of paste samples exposed to AMBT condition

3.5 Microstructure analysis by SEM and EDS

Figure 8(a) shows the microstructure of the sample OPC100. The specimen showed an expansion of 0.66%. Several micro cracks around the aggregate, as well as some cracks across the aggregate can be seen in this SEM image. The presence of ASR gels of fibrous morphology can be noticeable on the aggregate surface, in the cracks of aggregates and in pores of the binder matrix. Similar morphologies of ASR products has been well documented in the literature [37, 38]. These cracks in aggregates are associated to the aggregate dissolution due to the alkali attack from the binder matrix. ASR gel filled the cracks, absorbed moisture from the surroundings and expanded to increase the crack width. The cracks developed around the slag aggregate and extended to the aggregate cross-section, and therefore caused expansion and cracking of the specimens. The EDS analysis of ASR gel of OPC100 is given in **Figure 8(b)**. It can be seen that the ASR gel consists of silicon, calcium, sodium and potassium. The presence of magnesium is noticeable due to the magnesium content of FNS aggregate.

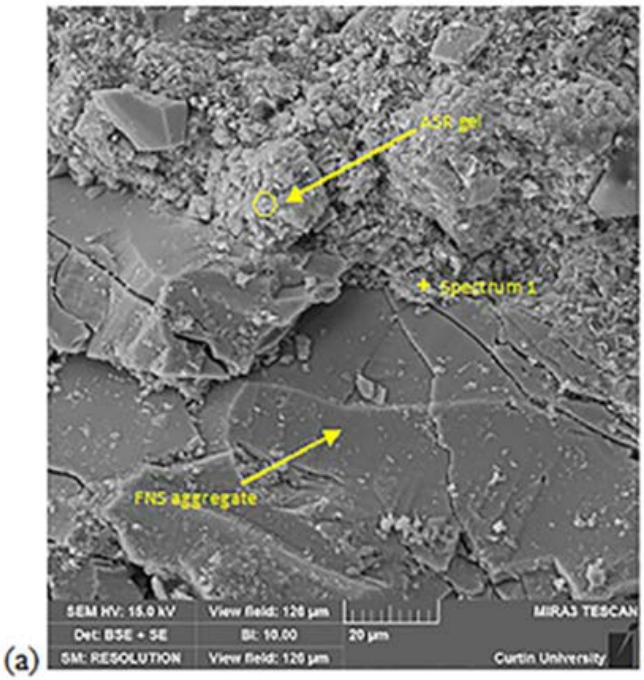
ASR gel
Spectrum 1
FNS aggregate
SEM HV: 15.0 kV
View field: 126 µm
MIRA3 TESCAN
Det: BSE + SE
BI: 10.00
20 µm
SM: RESOLUTION
View field: 126 µm
Curtin University

(a)

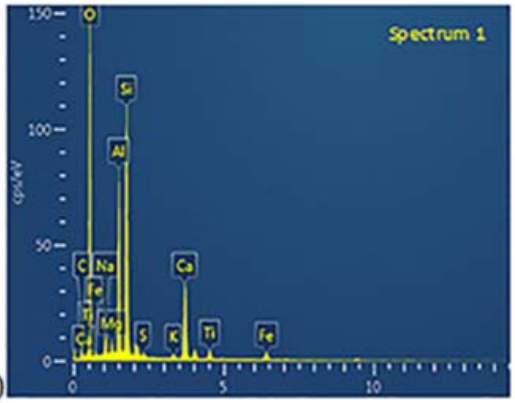
Spectrum 1
O
Si
Al
C
Na
Fe
Ti
Mg
Ca
S
K
Ti
Fe
cps/eV

(b)

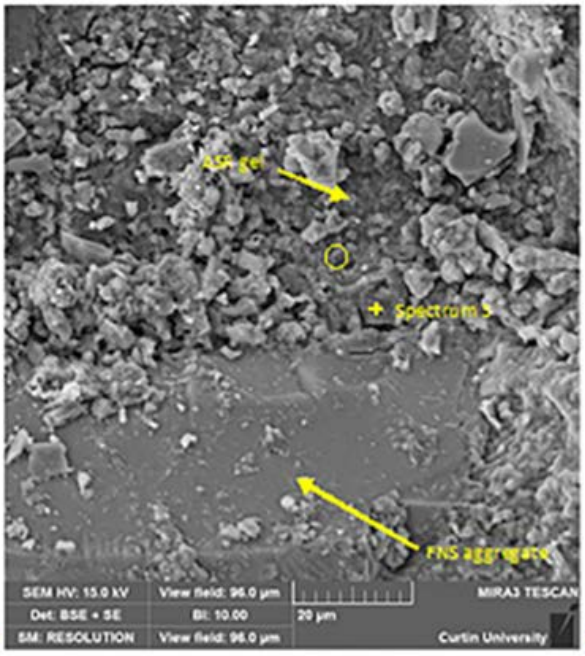
ASR gel
Spectrum 3
FNS aggregate
SEM HV: 15.0 kV
View field: 96.0 µm
MIRA3 TESCAN
Det: BSE + SE
BI: 10.00
20 µm
SM: RESOLUTION
View field: 96.0 µm
Curtin University

(e)

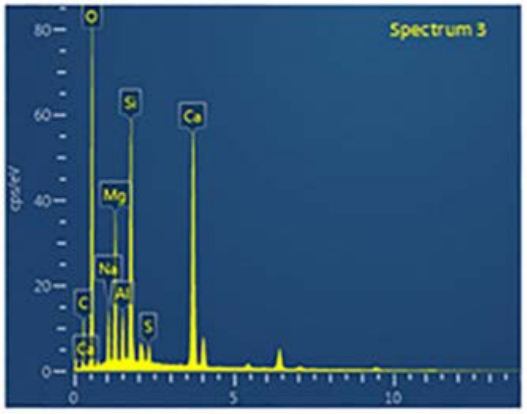
Spectrum 3
O
Si
Ca
Mg
Na
Al
C
S
Ca
cps/eV

(f)

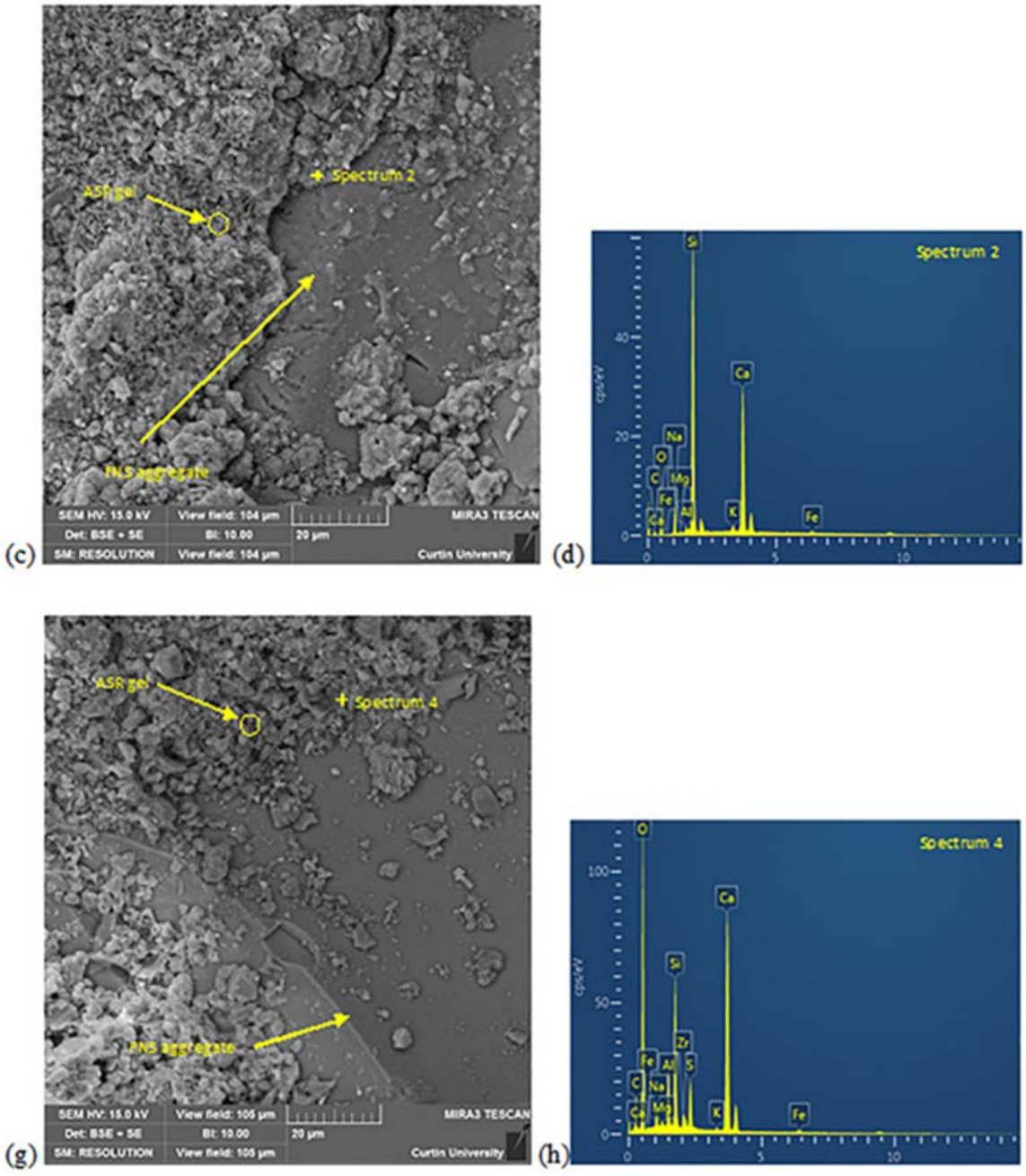

Figure 8 SEM and EDS of specimens after 21 days of NaOH exposure

Figure 8(c) shows an image of the sample of FA10. Formation of cracks due to ASR gel in the FNS aggregate surface can be seen in this figure. In addition, these gels also accumulated in the cracks of the aggregates and induced swelling pressure. The generation of small cracks filled with ASR gel are also noticeable in the cross-section of the aggregates. The chemical analysis of the gels in the cracks, as presented in **Figure 8(d)**, shows the presence of silicon, calcium, aluminium, sodium, potassium and magnesium. The presence of aluminium is due to the use of fly ash. However, the number of cracks and crack width in this specimen are less than those in OPC100.

The microstructural image of the sample containing 20% fly ash as SCM is presented in **Figure 8(e)**. It is noticeable that the aggregates suffered minor disintegration due to alkali attack. Very thin cracks can be observed at the interface of FNS aggregate and binder matrix which indicates significantly less ASR in the FA20 specimen as compared to the OPC100 and FA10 specimens. Also, no cracks were observed in the aggregate.

EDS in the cracks, as given in **Figure 8(f)**, shows that the gel consisted of high calcium/silicon ratio as compared to those of OPC100 and FA10. This phenomenon of high calcium/silicon ratio in ASR gel was attributed due to the presence of fly ash, which reduces the aggregate dissolution thus minimize the silica content from the ASR gel. The ASR gel with high Ca/Si ratio has a low swelling pressure. Therefore, this ASR gel caused less cracking in the microstructure of the specimen. Gholizadeh-Vayghan & Rajabipour [39] synthesised ASR gels consisting of different Ca/Si ratios and found that ASR gel with high Ca/Si had a low swelling pressure that can be dispersed in the microstructure. On the other hand, ASR gel with low Ca/Si has the affinity to absorb moisture and provide swelling pressure to the surrounding environment.

The SEM image of samples with 30% fly ash (FA30) is given in **Figure 8(g)**. It can be seen that the aggregate surface exhibits a firm bonding with the binder matrix. No cracking was observed on the aggregate, which indicates that the FNS aggregate in FA30 specimens had very minor dissolution. Furthermore, a negligible amount of ASR gels were observed on the aggregate surface. EDS analysis of the ASR gel on aggregate surface point out the gels consisting of high Ca/Si ratio. Therefore, due to the high Ca/Si ratio, the ASR gel did not impart swelling pressure to cause cracking.

4 Discussion

It is evident from the presented test results that expansion of the mortar specimens decreased with the increase of fly ash, and 30% fly ash was found to reduce the expansion below the 10-day and 21-day AMBT limits of the Australian Standard. The effectiveness of fly ash to reduce the ASR expansion is attributed to different reasons. First, the alkalinity of pore solution is reduced by fly ash. The fly ash contained very low amount of calcium oxide, which is only 0.6% by mass. Thus, the total alkalinity of the binder decreased with the increase of fly ash as cement replacement. The increase of the low-calcium fly ash as cement replacement reduced the amount of Portlandite generated by the hydration of cement. The subsequent pozzolanic reaction of fly ash further consumed Portlandite. The presented TGA results confirmed the reduction of Portlandite by fly ash. Therefore, fly ash as a SCM reduced the overall alkalinity of pore solution that reduced the ASR of FNS aggregate.

Secondly, fly ash helped by reducing the permeability of the binder matrix. The presented VPV test results show that porosity decreased with the increase of fly ash. The densification of the binder matrix by fly ash resulted in an increase of strength at a higher rate with the increase of age as compared to the control mix. Therefore, the internal voids are filled by the secondary C-S-H gel produced by fly ash [40]. The accelerated mortar bar test exposure involves immersion of the specimen in an alkaline solution. The reduction of permeability by fly ash helped reduce ingress of alkaline solution from outside of the sample. This helped to reduce the ASR of FNS in the AMBT condition.

Finally, fly ash also helped with the ASR gel modification. Fly ash is found to react with the alkali silicate gel and change the gel properties. The EDS analysis was carried out to determine the Ca/Si ratio of products for all four samples and the values were 1.78, 2.18, 2.46 and 2.63 for OPC100, FA10, FA20 and FA30, respectively. Thus, the Ca/Si ratio of the ASR

gel gradually increased with the increase of fly ash. Therefore, the modified ASR gel generated low swelling pressure that did not cause severe internal cracking on the aggregate surface. As a result, specimens containing 20% and 30% fly ash did not exhibit any cracking on the aggregate surface even after an extended period of the accelerated mortar bar test.

5 Conclusions

The effect of fly ash on ASR expansion of by-product FNS fine aggregate was studied by accelerated mortar bar tests. The fine aggregate of the mortar bar specimens consisted of 50% FNS and 50% natural sand. A class F fly ash was used as 10%, 20% and 30% replacement of cement. The following conclusions are drawn from the study:

1. Expansion of mortar bar specimens decreased with the increase of fly ash in the accelerated test condition. According to the 10-day and 20-day expansion limits of the Australian Standard, the mortar bar specimens were classified as reactive, slowly reactive and non-reactive for the fly ash contents of 10%, 20% and 30%, respectively.
2. Surface cracks were observed in the specimens using no fly ash and 10% fly ash. There was no surface cracks in the specimens using 20% and 30% fly ash.
3. The volume of permeable voids decreased from 18% to 14% by the use of 30% fly ash which shows densification of the binder matrix by pozzolanic reaction of fly ash.
4. The TGA results showed that Portlandite content of paste samples exposed to AMBT condition decreased from 4.25% to 1.36% by the use of 30% fly ash.
5. The Ca/Si ratio of the ASR product increased from 1.78 to 2.63 by the use of 30% fly ash. This shows a modification of the ASR product by fly ash.
6. Overall, fly ash reduced the ASR expansion of FNS aggregates by reduction of the alkalinity of pore solution, densification of the binder matrix by pozzolanic reaction and modification of the ASR gel to cause less swelling pressure and cracking.
7. Therefore, the use of FNS aggregate and fly ash can be considered as a feasible option for production of technically sound and environmentally friendly concrete.

Acknowledgement

The authors acknowledge the contribution and support of SLN, New Caledonia through its research department. The authors are also thankful to Microscopy and Microanalysis Facility - John de Laeter Centre, Curtin University for their support.

References

1. Ghods, P., Alizadeh, R., & Salehi, M. (2017). Electrical methods and systems for concrete testing. *U.S. Patent No. 9,638,652*. Washington, DC: U.S. Patent and Trademark Office.
2. Davis, J., Bird, J., Finlayson, B., & Scott, R. (2000). The management of gravel extraction in alluvial rivers: a case study from the Avon River, southeastern Australia. *Physical Geography*, 21(2), 133-154. doi:10.1080/02723646.2000.10642703
3. Padmalal, D., Maya, K., Sreebha, S., & Sreeja, R. (2008). Environmental effects of river sand mining: a case from the river catchments of Vembanad lake, Southwest coast of India. *Environmental geology*, 54(4), 879-889. doi:10.1007/s00254-007-0870-z
4. Van Den Berg, J. H., Van Gelder, A., & Mastbergen, D. R. (2002). The importance of breaching as a mechanism of subaqueous slope failure in fine sand. *Sedimentology*, 49(1), 81-95. doi:10.1111/j.1525-139X.2006.00168.x-i1
5. Sajinkumar, K. S., Sankar, G., Rani, V. R., & Sundarajan, P. (2014). Effect of quarrying on the slope stability in Banasuramala: an offshoot valley of Western Ghats, Kerala, India. *Environmental earth sciences*, 72(7), 2333-2344. doi:10.1007/s12665-014-3143-7
6. Giebson, C., Voland, K., Ludwig, H. M., & Meng, B. (2017). Alkali-silica reaction performance testing of concrete considering external alkalis and preexisting microcracks. *Structural Concrete*, 18(4), 528-538. doi: 10.1002/suco.201600173
7. Wiedmann, A., Weise, F., Kotan, E., Müller, H. S., & Meng, B. (2017). Effects of fatigue loading and alkali–silica reaction on the mechanical behavior of pavement concrete. *Structural Concrete*, 18(4), 539-549. doi: 10.1002/suco.201600179
8. Stanton, T.E. (1940). Expansion of concrete through reaction between cement and aggregate. *Proc Am Soc Civil Eng*, 66(10), 1781–811.
9. Berra, M., Mangialardi, T., Paolini, A. E., & Turriziani, R. (1991). Critical evaluation of accelerated test methods for detecting the alkali-reactivity of aggregates. *Advances in Cement Research*, 4(13), 29-37. doi:10.1680/adcr.1991.4.1.29
10. Na, O., Xi, Y., Ou, E., & Saouma, V. E. (2016). The effects of alkali-silica reaction on the mechanical properties of concretes with three different types of reactive aggregate. *Structural Concrete*, 17(1), 74-83. doi:10.1002/suco.201400062
11. Saha, A. K., & Sarker, P. K. (2016). Expansion due to alkali-silica reaction of ferronickel slag fine aggregate in OPC and blended cement mortars. *Construction and Building Materials*, *123*, 135-142. doi:10.1016/j.conbuildmat.2016.06.144
12. Glasser FP (1992) Chemistry of the alkali aggregate reaction. In: R.N. Swamy (ed) *The Alkali–Silica Reaction in Concrete*, Blackie, Glasgow and London, and Van Nostrand-Reinhold, New York, pp 30–53
13. Ichikawa, T., & Miura, M. (2007). Modified model of alkali-silica reaction. *Cement and Concrete research*, 37(9), 1291-1297. doi:10.1016/j.cemconres.2007.06.008
14. Chatterji, S. (1979). The role of Ca $(OH)_2$ in the breakdown of Portland cement concrete due to alkali-silica reaction. *Cement and concrete research*, 9(2), 185-188. doi:10.1016/0008-8846(79)90024-3
15. Dron, R., & Brivot, F. (1993). Thermodynamic and kinetic approach to the alkali-silica reaction. Part 2: Experiment. *Cement and Concrete Research*, 23(1), 93-103. doi:10.1016/j.cemconres.2010.11.003

16. Matos, A. M., & Sousa-Coutinho, J. (2016). ASR and sulphate performance of mortar containing industrial waste. *Structural Concrete*, 17(1), 84-95. doi:10.1002/suco.201400095
17. Thomas, M. (2011). The effect of supplementary cementing materials on alkali-silica reaction: A review. *Cement and Concrete Research*, 41(12), 1224-1231. doi:10.1016/j.cemconres.2010.11.003
18. Thomas, M. D. A. (1996). *Review of the effect of fly ash and slag on alkali-aggregate reaction in concrete*. Building Research Establishment Report, BR314, Construction Research Communications, Watford, UK, 1996.
19. Shehata, M. H., Thomas, M. D., & Bleszynski, R. F. (1999). The effects of fly ash composition on the chemistry of pore solution in hydrated cement pastes. *Cement and Concrete Research*, 29(12), 1915-1920. doi:10.1016/S0008-8846(99)00190-8
20. Shehata, M. H., & Thomas, M. D. (2002). Use of ternary blends containing silica fume and fly ash to suppress expansion due to alkali–silica reaction in concrete. *Cement and Concrete Research*, 32(3), 341-349. doi:10.1016/S0008-8846(01)00680-9
21. Turk, K., Kina, C., & Bagdiken, M. (2017). Use of binary and ternary cementitious blends of F-Class fly-ash and limestone powder to mitigate alkali-silica reaction risk. *Construction and Building Materials*, 151, 422-427. doi:10.1016/j.conbuildmat.2017.06.075
22. Du, C. (2005). A review of magnesium oxide in concrete. *Concrete international*, 27(12), 45-50.
23. Rahman, M. A., Sarker, P. K., Shaikh, F. U. A., & Saha, A. K. (2017). Soundness and compressive strength of Portland cement blended with ground granulated ferronickel slag. *Construction and Building Materials*, 140, 194-202. doi:10.1016/j.conbuildmat.2017.02.023
24. Saha, A. K., & Sarker, P. K. (2017a). Sustainable use of ferronickel slag fine aggregate and fly ash in structural concrete: Mechanical properties and leaching study. *Journal of Cleaner Production*, 162(20), 438-448. doi:10.1016/j.jclepro.2017.06.035
25. Saha, A. K., & Sarker, P. K. (2017b). Compressive strength of mortar containing ferronickel slag as replacement of natural sand. *Procedia Engineering*, 171, 689-694. doi:10.1016/j.proeng.2017.01.410
26. AS 1141.60.1 (2014). Method for Sampling and Testing Aggregates, Potential Alkali Silica Reactivity – Accelerated Mortar Bar Method. *Standards Australia*, Sydney, Australia.
27. ASTM C642 (2006). Standard test method for density, absorption, and voids in hardened concrete. West Conshohocken, Pennsylvania, United States.
28. Andrews-Phaedonos, F. (1996). Establishing the durability performance of structural concrete. VicRoads, Melbourne, Australia, 79.
29. Nixon, P. J., & Sims, I. (2016). RILEM Recommended Test Method: AAR-2—Detection of Potential Alkali-Reactivity—Accelerated Mortar-Bar Test Method for Aggregates. In: Nixon P., Sims I. (eds) *RILEM Recommendations for the Prevention of Damage by Alkali-Aggregate Reactions in New Concrete Structures.* RILEM State-of-the-Art Reports, vol 17. Springer, Dordrecht. Doi: 10.1007/978-94-017-7252-5_4
30. ASTM C1567 (2013). Standard Test Method for Determining the Potential Alkali-Silica Reactivity of Combinations of Cementitious Materials and Aggregate (Accelerated Mortar-Bar Method). West Conshohocken, Pennsylvania, United States.
31. Aly, M., Hashmi, M. S. J., Olabi, A. G., Messeiry, M., Abadir, E. F., & Hussain, A. I. (2012). Effect of colloidal nano-silica on the mechanical and physical behaviour of

waste-glass cement mortar. *Materials & Design*, 33, 127-135. doi:10.1016/j.matdes.2011.07.008
32. Chappex, T., & Scrivener, K. (2012). Alkali fixation of C–S–H in blended cement pastes and its relation to alkali silica reaction. *Cement and Concrete Research*, 42(8), 1049-1054. doi:10.1016/j.cemconres.2012.03.010
33. Esteves, L. P. (2011). On the hydration of water-entrained cement–silica systems: combined SEM, XRD and thermal analysis in cement pastes. *Thermochimica Acta*, 518(1), 27-35. doi:10.1016/j.tca.2011.02.003
34. Frías, M., & Cabrera, J. (2001). Influence of MK on the reaction kinetics in MK/lime and MK-blended cement systems at 20 C. *Cement and concrete research*, 31(4), 519-527. doi:10.1016/S0008-8846(00)00465-8
35. Vedalakshmi, R., Raj, A. S., Srinivasan, S., & Babu, K. G. (2003). Quantification of hydrated cement products of blended cements in low and medium strength concrete using TG and DTA technique. *Thermochimica Acta*, 407(1), 49-60. doi:10.1016/S0040-6031(03)00286-7
36. Shui, Z. H., Zhang, R., Chen, W., & Xuan, D. X. (2010). Effects of mineral admixtures on the thermal expansion properties of hardened cement paste. *Construction and Building Materials*, 24(9), 1761-1767. doi:10.1016/j.conbuildmat.2010.02.012
37. Beglarigale, A., & Yazici, H. (2013). Mitigation of detrimental effects of alkali-silica reaction in cement-based composites by combination of steel microfibers and ground-granulated blast-furnace slag. *Journal of Materials in Civil Engineering*, 26(12), 04014091. doi:10.1061/(ASCE)MT.1943-5533.0001005
38. Yazici, H. (2012). The effect of steel micro-fibers on ASR expansion and mechanical properties of mortars. *Construction and Building Materials*, 30, 607-615. doi:10.1016/j.conbuildmat.2011.12.051
39. Gholizadeh-Vayghan, A., & Rajabipour, F. (2017). The influence of alkali–silica reaction (ASR) gel composition on its hydrophilic properties and free swelling in contact with water vapor. *Cement and Concrete Research*, 94, 49-58. doi:10.1016/j.cemconres.2017.01.006
40. Ghrici, M., Kenai, S., & Said-Mansour, M. (2007). Mechanical properties and durability of mortar and concrete containing natural pozzolana and limestone blended cements. *Cement and Concrete Composites*, 29(7), 542-549. doi:10.1016/j.cemconcomp.2007.04.009